Green Plant Photosystem I Binds Light-Harvesting Complex I on One Side of the Complex†

Egbert J. Boekema,‡ Poul Erik Jensen,§ Eberhard Schlodder,|| Jan F. L. van Breemen,‡ Henny van Roon,⊥ Henrik Vibe Scheller,§ and Jan P. Dekker*,⊥

Groningen Biotechnology and Biomolecular Sciences Institute, University of Groningen, Nijenborgh 4, 9747 AG Groningen, The Netherlands, Plant Biochemistry Laboratory, Department of Plant Biology, The Royal Veterinary and Agricultural University, 40 Thorvaldsensvej, DK-1871 Frederiksberg C, Copenhagen, Denmark, Max Volmer Institute of Biophysical Chemistry and Biochemistry, Technische Univerität Berlin, Strasse des 17. Juni 135, D-10623 Berlin, Germany, and Department of Physics and Astronomy, Institute of Molecular Biological Sciences, Vrije Universiteit, De Boelelaan 1081, 1081 HV Amsterdam, The Netherlands

Received July 5, 2000; Revised Manuscript Received November 6, 2000

ABSTRACT: We report a structural characterization by electron microscopy of green plant photosystem I solubilized by the mild detergent *n*-dodecyl-α-D-maltoside. It is shown by immunoblotting that the isolated complexes contain all photosystem I core proteins and all peripheral light-harvesting proteins. The electron microscopic analysis is based on a large data set of 14 000 negatively stained single-particle projections and reveals that most of the complexes are oval-shaped monomers. The monomers have a tendency to associate into artificial dimers, trimers, and tetramers in which the monomers are oppositely oriented. Classification of the dimeric complexes suggests that some of the monomers lack a part of the peripheral antenna. On the basis of a comparison with projections from trimeric photosystem I complexes from cyanobacteria, we conclude that light-harvesting complex I only binds to the core complex at the side of the photosystem I F/J subunits and does not cause structural hindrances for the type of trimerization observed in cyanobacterial photosystem I.

Photosystem I (PSI)[1] is a large supramolecular pigment−protein complex embedded in the thylakoid membranes of organisms performing oxygenic photosynthesis (*1*). Its main component is the so-called reaction center core complex, which contains all the reactants required for the plastocyanin−ferredoxin oxidoreductase function and binds about 100 chlorophyll *a* antenna molecules. In cyanobacteria the PSI core complex consists of 11 proteins designated PSI-A to PSI-F and PSI-I to PSI-M. Most of these proteins have one or more membrane-spanning α-helices, but PSI-C to PSI-E are extrinsically located at the stromal side of the thylakoid membrane. The total protein mass of this complex is about 260 kDa, of which about 37 kDa originates from the three extrinsic proteins. The structure of the core complex of the cyanobacterium *Synechococcus elongatus* has been resolved at 4 Å resolution by X-ray crystallography (*2*, *3*) and reveals 43 α-helices (of which 31 span the thylakoid membrane) and 89 chlorophylls (of which six could be identified as special reaction center components). Cyanobacterial PSI has been shown to exist in monomeric and trimeric forms, both in the membrane (*4*) and after detergent isolation (*5*, *6*). It is not understood very well why the possibility for PSI to occur in two different aggregation forms would be advantageous for cyanobacteria. It has been suggested that the trimeric form could have an increased affinity for the phycobilisomes and that an interchange between the monomeric and trimeric form could be one of the manifestations of the state transitions in cyanobacteria (*7*). It is also possible that the sometimes observed increased amount of long-wavelength antenna pigments in the trimeric form could protect the photosystem under certain stress conditions (*8*).

The structure of the PSI core complex from higher plants is not known in much detail. This complex does not contain PSI-M (∼3 kDa) but instead contains PSI-G, PSI-H, and PSI-N (10−11 kDa each), which are not found in cyanobacteria. The PSI-N subunit is extrinsically located at the lumenal surface of the complex, whereas PSI-G and PSI-H most likely have one or two transmembrane α-helices (*1*). Studies by electron microscopy of negatively stained specimens revealed very similar structures (at ∼20 Å resolution) of the core parts of higher plant (*9*, *10*) and cyanobacterial (*5*, *6*) PSI, suggesting that the slightly different polypeptide composition does not cause pronounced structural differences at this resolution.

PSI from green plants and green algae binds a number of additional light-harvesting pigment-binding proteins belong-

† This research was supported by The Netherlands Foundation for Scientific Research via the Foundation for Life and Earth Sciences (E.J.B. and J.P.D.), by the Danish National Research Foundation (P.E.J. and H.V.S.), and by the Deutsche Forschungsgemeinschaft, Sfb 498, TP A1 (E.S.).

* To whom correspondence should be addressed: Telephone +31 20 4447931; fax +31 20 4447999; e-mail dekker@nat.vu.nl.

‡ University of Groningen.

§ Royal Veterinary and Agricultural University.

|| Technische Universität Berlin.

⊥ Vrije Universiteit Amsterdam.

[1] Abbreviations: α-DM, *n*-dodecyl-α-D-maltoside; *β*-DM, *n*-dodecyl-*β*-D-maltoside; Cab, chlorophyll *a/b* binding protein; Chl, chlorophyll; EM, electron microscopy; LHCI, light-harvesting complex I; P700, primary electron donor of PSI; PSI, photosystem I.

10.1021/bi0015358 CCC: $20.00
Published on Web 12/30/2000

ing to the family of nuclear-encoded Cab proteins. These proteins are generally referred to as light-harvesting complex I (LHCI) and contain together up to 100 additional chlorophyll *a* + *b* antenna molecules. LHCI is known to consist of four proteins called Lhca1−4, which have protein masses of about 20−24 kDa and are present in approximately equal amounts (*11*). Lhca1 and Lhca4 have been shown to form a heterodimer in vivo (*12*, *13*), while Lhca2 and Lhca3 may associate in hetero- and/or homodimers (*14*−*16*). The amino acid sequences of all LHCI proteins show strong similarities with that of LHCII, the structure of which has been resolved by electron crystallography at 4 Å resolution (*17*).

Information on the structural organization of LHCI and the PSI core in the native green plant PSI complex (generally referred to as PSI-200) has been obtained from electron microscopy by single-particle analysis (*18*) and from cross-linking studies (*14*). The latter studies also revealed that the various LHCI subunits associate with the PSI core complex independently of each other. These studies led to the idea that the PSI core complex is completely surrounded by a monolayer of eight LHCI monomers (*18*) or almost completely surrounded by four LHCI dimers (*14*). There are no indications that the green plant PSI complex can occur in trimers, despite the presence of the PSI-L subunit (*19*). A very homologous form of this hydrophobic protein exists in cyanobacteria (*20*), where it has been shown to be required for trimer formation (*21*). It is possible that the binding of LHCI to the PSI core creates a steric barrier for the trimerization.

In this work we reinvestigate the supramolecular organization of green plant PSI and present an elaborate study of PSI complexes obtained by a treatment of spinach thylakoids by the very mild detergent *n*-dodecyl-α-D-maltoside (α-DM). We show that the isolated PSI complexes can occur in monomeric, dimeric, trimeric, and even higher association forms with similar protein compositions. Electron microscopy and single-particle image analysis of a large data set of more than 14 000 projections of negatively stained specimens reveals that various aggregation forms are artificial, that LHCI occurs only on one side of the complex (the one occupied by the PSI-F, PSI-J, and PSI-E subunits), and that the binding of LHCI to the PSI core complex will not prevent a similar type of trimerization as observed in cyanobacteria.

MATERIALS AND METHODS

Sample Preparation. PSI-200 complexes were isolated from thylakoid membranes from market spinach as described by Van Roon et al. (*22*). In short, the thylakoids (at a final chlorophyll concentration of 1.4 mg/mL) were suspended in a buffer containing 20 mM BisTris (pH 6.5) and 5 mM $MgCl_2$, partially solubilized with α-DM (final concentration 1.2%), centrifuged for 3 min at 9000 rpm in an Eppendorf table centrifuge, pushed through a 0.45 μm filter to remove unsolubilized material, and partially purified by gel-filtration chromatography on a Superdex 200 HR 10/30 column (Pharmacia) with 20 mM BisTris (pH 6.5), 5 mM $MgCl_2$, and 0.03% α-DM as mobile phase. The chromatography was carried out at room temperature with a flow rate of 25 mL/h. After the appearance of the first green material, at 16.3 min after the solubilized thylakoids were supplied to the gel-filtration column, up to 14 fractions of 0.6 mL each were collected (*22*) and either kept at 4 °C and analyzed by electron microscopy within 1 h or frozen for a later biochemical or immunological analysis. The fractions from this procedure were designated fractions 1−14 as in ref *22*. In some cases, the chromatography was performed with two Superdex 200 HR 10/30 columns connected in series, with identical buffer composition, flow rate, and other conditions and further handling of the samples as described above with the single gel-filtration chromatography step. The fractions obtained with this procedure (again 0.6 mL each) were designated fraction a (eluting from 33.0 to 34.5 min) to fraction x (eluting from 67.5 to 69 min).

Biochemical Characterization. Chlorophyll *a* and *b* contents were measured in 80% acetone by use of the extinction coefficients reported by Porra et al. (*23*). The content of P700 was determined by flash-induced absorbance changes in the red and infrared parts of the spectrum (*24*). Immunoblotting was performed on representative fractions from the gel-filtration chromatography steps. Proteins were separated by SDS−PAGE and transferred to nitrocellulose membranes followed by incubation with primary antibodies raised against the barley PSI core subunits PSI-C, -D, -E, -F, -G, -H, -K, -L, and -N and the four Lhca proteins. The interaction between primary antibodies and PSI proteins was visualized by use of secondary antibodies conjugated with horseradish peroxidase (Dako, Copenhagen, Denmark) and a chemiluminescent detection system (ECL, Amersham, U.K.) according to the instructions of the manufacturer. The Lhca1 and Lhca3 antibodies were a kind gift from Dr. Stefan Jansson, University of Umeå (Sweden).

Electron Microscopy. Transmission electron microscopy was performed with a Philips CM10 electron microscope at 52000× magnification. Negatively stained specimens were prepared on glow-discharged carbon-coated copper grids as in ref *25*. Micrographs were digitized with a Kodak Eikonix Model 1412 CCD camera with a step size of 25 μm, corresponding to a pixel size of 0.485 nm at the specimen level. Projections were extracted for image analysis with IMAGIC software (*26*) following alignment procedures and treatment by multivariate statistical analysis and classification as described previously (*25*−*27*).

RESULTS

Sample Preparation. Incubation of thylakoid membranes from spinach with α-DM in the presence of 5 mM $MgCl_2$ resulted in a selective solubilization of the stromal parts of the membrane (*22*). Under these conditions, the grana membranes remained intact and PSI and other solubilized complexes could be separated from these large membrane fractions by a single gel-filtration chromatography step. In ref *22* it was shown by pigment analysis, SDS−PAGE, absorption spectra at room temperature, and emission spectra at 4 K that fractions 3−6 from the single chromatography experiment were strongly enriched in PSI, although fraction 3 was contaminated with PSII (mainly small grana membrane fragments) and fractions 5 and 6 were heavily contaminated with the CF_oF_1 ATP synthase complex.

Figure 1 (solid line) shows a typical chromatogram of the double-column procedure, recorded at 400 nm. As in the case of the single-column procedure (*22*), six main fractions are observed; however, they are much better separated. The A_{700}/

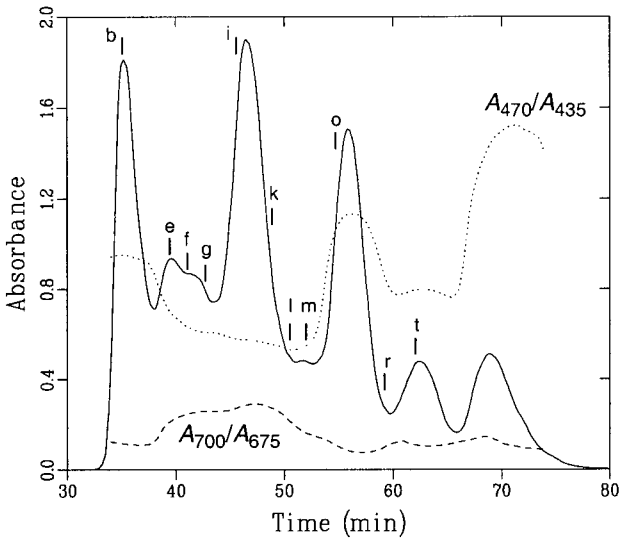

FIGURE 1: FPLC gel-filtration chromatogram (solid line), recorded at 400 nm, of spinach thylakoid membranes solubilzed with α-DM, obtained from two Superdex 200 HR 10/30 columns connected in series. The chromatogram is plotted together with the A_{700}/A_{675} ratio (dashed line) and the A_{470}/A_{435} ratio (dotted line) to get information on the relative contents of the long-wavelength antenna chlorophylls and Chl *b* + carotenoids, respectively. The values on the *y*-axis are the real values of these ratios. The flow rate was 25 mL/h. The fractions designated b−t correspond with those analyzed in Figure 2.

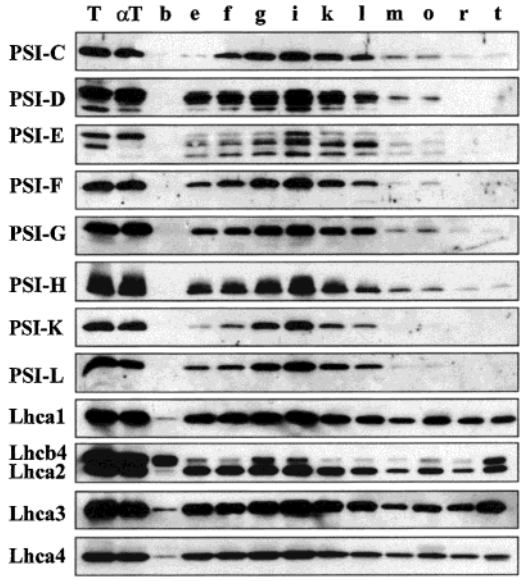

FIGURE 2: Immunoblot analysis of fractins b−t from the two-column gel-filtration chromatography procedure (see Figure 1), loaded on SDS−polyacrylamide gels in equal volumes. The lanes designated T and αT represent the original thylakoid membranes and the α-DM-solubilized fraction of these thylakoids, resectively. The blots were incubated with antibodies against PSI core and LHCI proteins as indicated.

A_{675} ratio (dashed line) indicates that PSI elutes in two main fractions after about 40 and 46 min in fractions e and i, respectively. We will show in the following that the fraction eluting after 46 min originates from monomeric PSI-200 particles and that in the fractions eluting at earlier times several higher association forms of PSI-200 are present.

Immunological Characterization. We performed an immunological analysis of the main fractions from the gel-filtration chromatography in order to determine the relative contents of the various PSI subunits. The analysis was done on fractions from both the double-column procedure (because with this procedure the monomers and higher association forms were much better separated) and the single-column procedure (because the EM experiments were performed on fractions obtained with this procedure). Figure 2 shows that the main fraction of PSI from the double-column procedure (fraction i) contains all PSI core and LHCI proteins and that the higher molecular-mass particles in fractions e and f also contain all PSI core and LHCI proteins. This suggests that the various PSI aggregation forms have identical protein compositions. We note that in the case of the PSI-E protein a number of breakdown products are observed in the chromatography fractions but not in the starting materials (T and αT), whereas the PSI-N protein did not show any response in any of the chromatography fractions but was clearly present in both starting materials (not shown). The breakdown of both proteins is probably induced by the overnight storage at 4 °C of these particular samples, because similar experiments on quickly frozen samples (from the single-column procedure) did not reveal any PSI-E breakdown product and also showed the presence of PSI-N in fractions 3−7, which roughly correspond to fractions e−k from the double-column procedure. We also note that the relatively weak staining in Figure 2 of the PSI-C and PSI-K subunits in fractions e and f, and to a lesser extent also of PSI-L and PSI-F, is an artifact caused a combination of a relatively weak antibody and a low protein concentration in these fractions. The application of larger amounts of sample (from the single-column procedure) resulted in disproportionally larger amounts of stain of these antibodies, while the Coomassie brilliant blue (CBB) staining patterns of the monomeric and oligomeric PSI fractions were similar (data not shown). The analysis in Figure 2 also shows that the largest fraction (b) does not contain any PSI protein, which is not surprising if this fraction consists of PSII membrane fragments (*22*). The presence of PSII in this fraction is confirmed by the Lhca2 antibody, because this antibody also detects the Lhcb4 (CP29) protein of PSII, which migrates slightly slower on SDS−PAGE than the Lhca2 protein (Figure 2).

It is furthermore of interest to note that the fractions o, r, and t (in which, respectively, trimeric, dimeric, and monomeric LHC complexes should be maximally present) do not show a significant response to antibodies against any of the PSI core subunits but do show a clear response to those of all four LHCI proteins. Very similar results were obtained with the samples from the one-column procedure (not shown). These results suggest that a rather unspecific part of the LHCI antenna is detached from the PSI core complex during solubilization of the membranes and/or the chromatography or that there is a pool of unconnected LHCI in the thylakoid membranes.

To estimate the amount of unconnected LHCI protein, we performed a number of serial dilution experiments with the Lhca2 and Lhca4 antibodies. Figure 3 shows the results for fractions 5 and 10 of the single-column procedure, which are most enriched in monomeric PSI-200 complexes and dimeric LHCI complexes, respectively (*22*). The results indicate that Lhca4 and Lhca2 are 10−20 and 5−10 times

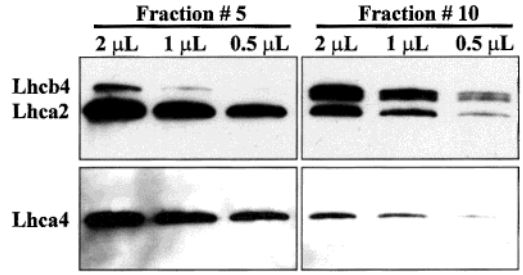

FIGURE 3: Immunoblot analysis of various dilutions of fractions 5 and 10 from the one-column gel-filtration chromatography procedure to get an indication of the LHCI content of these fractions. The blotted proteins were developed with antibodies against the Lhca2 and Lhca4 proteins.

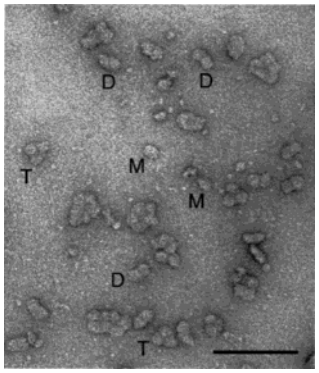

FIGURE 4: Part of an electron micrograph showing various types of PSI complexes, negatively stained with 2% uranyl acetate. Some monomeric (M), dimeric (D), and trimeric (T) PSI particles have been indicated. The scale bar equals 100 nm.

more abundant in fraction 5 than in fraction 10, suggesting that only a relatively small portion of LHCI is not bound to the PSI core complex. The same was concluded from an analysis of the fluorescence properties of the various fractions (*22*). Figure 3 also shows that the Lhcb4 protein of PSII (CP29) is more abundant in fraction 10 than in fraction 5.

Antenna Size. We performed flash-induced absorbance-difference measurements between 661 and 730 nm and at 826 nm to estimate the concentration of P700 in a sample with the combined fractions 5 and 6 from the single-column procedure, and compared the results with those obtained with a PSI-200 preparation isolated with β-DM (*28*). In the red wavelength region, the absorbance-difference spectrum attributed to the oxidation of P700 was for both preparations almost identical to the spectra reported before for spinach (*29*) and *Synechococcus* (*30*) PSI preparations. The maximum bleaching in the Q_y region at 703 nm corresponds to a differential extinction coefficient of 64 000 M^{-1} cm^{-1} for the spinach preparation (*29*) and a slightly lower value of 61 000 M^{-1} cm^{-1} for the *Synechococcus* preparation (C. Flemming and E. Schlodder, unpublished observations). Assuming a differential extinction coefficient between these values for the PSI-200 preparations, the flash-induced absorbance changes at 703 nm revealed antenna sizes of 196 $\pm$ 7 and 175 $\pm$ 7 Chl ($a + b$) per P700 for the α-DM and β-DM preparations, respectively. The measurements at 826 nm gave the same results, with a differential extinction coefficient of 7500 M^{-1} cm^{-1}. We note that similar experiments revealed an antenna size of 102 $\pm$ 6 Chl *a* for trimeric PSI particles from *Synechococcus*, in reasonable agreement with the number of Chl *a* molecules identified in the crystal structure. The values of 175−200 Chl ($a + b$) per P700 agree with most estimates of the antenna size of the native PSI complex from higher plants (see, e.g., ref *31*). We note, however, that the value found for the α-DM preparation is somewhat overestimated because of the presence of PSII impurities (Figures 2 and 3) and that the values for both preparations may represent underestimations of the antenna size of the complete complex because of the partial absence of LHCI subunits (see also below). We conclude that the complete PSI-200 complex contains at least 180 Chl ($a + b$) per P700.

Electron Microscopy. Electron microscopy was performed on the fractions obtained after a single gel-filtration chromatography step. For this technique, a high degree of purification is not required, since impurities are effectively recognized and separated by the classification procedures of the various types of particle projections. A good example of the strength of this technique was presented in ref *32*, where new characteristic PSII−LHCII supercomplexes could be observed in a nonpurified set of complexes obtained by partial solubilization of PSII membranes.

A part of an electron micrograph of fraction 3 is shown in Figure 4. It shows that a dimeric type of complex is relatively abundant in this fraction but that trimers and even larger aggregates are present as well. Fraction 3 showed small numbers of monomeric PSI complexes and was mostly free from CF_oF_1 ATPase complexes and totally free from dimeric PSII−LHCII supercomplexes. Only one C_2S_2 supercomplex (*25*) was observed during the particle selection of this fraction. Fractions 5 and 6 contained mainly monomeric PSI and ATP synthase complexes (not shown).

To obtain a reasonably sized data set of the α-DM solubilized PSI particles, we scanned 257 electron micrographs of fractions 3−6, yielding total numbers of 5001, 6683, 2000, and 436 monomeric, dimeric, trimeric, and tetrameric PSI particle projections, respectively. The same data set also gave a total of 17 300 projections from the ATPase complex. A detailed analysis of these projections has been presented elsewhere (*22*).

Monomers and Dimers. Image analysis of the projections was performed separately for the monomers, dimers, trimers, and tetramers by a combination of multivariate statistical analysis and classification. The classification of the 5001 monomeric projections showed only one predominant view (Figure 5F) with dimensions of 20 $\times$ 16 nm (including the detergent layer). The overall size and shape of these particles are identical to those of PSI-200 particles isolated previously in β-DM (*18*). The present images (see Figure 6B for a contoured version) show, however, much more internal structure, such as two large stain-excluding masses in the upper part of the complex, three or four small stain-excluding masses in the lower part, and a very uneven stain distribution around the particle. The latter feature could be caused by the presence of a nearby extrinsic subunit that elevates the height of the particle.

The large data set of the dimers was initially decomposed into 36 classes. This number was large enough to comprise all possible types of projections but not too large given the size of the data set. Of the 36 classes, 25 showed images with well-preserved features, while the others were somewhat fuzzy but not very different otherwise. Of these 25 classes,

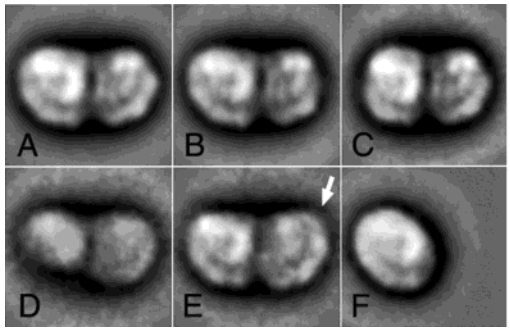

FIGURE 5: Image analysis of dimeric and monomeric PSI complexes. (A−C) Three most frequent views found by classification of 6683 dimeric projections. For these sums, 650, 400, and 257 well-preserved images were summed, respectively. (D, E) Rare views consisting of 88 and 98 summed projections. (F) Sum of the best 600 monomeric projections (out of 5000), shifted after analysis into a position equivalent to the left monomer in the dimer (A). The right monomer of the dimer is on the average embedded in a thicker layer of negative stain, except for the particles from the class in panel E, in which the upper right tip (white arrow) has about the same shape as in the left monomer.

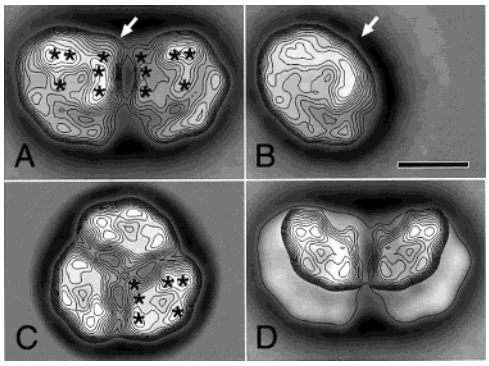

FIGURE 6: Comparison of monomeric and dimeric PSI-200 complexes with cyanobacterial PSI. (A, B) Contoured versions of the sums of Figure 5 panels A and F, respectively. The absence of a protruding density in the monomeric sum (B), consisting of at least the PSI-L subunit, is indicated by a white arrow. (C) Projection of trimeric PSI from *Synechocystis 6803* without the PSI-D/E subunits (*6*) of which the lower right monomer is brought into a position that is rotationally equivalent to the right dimer in (A). (D) Schematic of the green plant dimer in which the core part from the trimer is fitted into the dimer. The remaining densities in the lower half indicate the part in the complex occupied by LHCI subunits. Asterisks indicate positions of densities that are similar in panels A and C. Scale bar equals 10 nm.

13 classes were very similar, showing a predominant view that represents about 63% of the data set (Figure 5A). This view has maximal dimensions of 31 × 17 nm and its contoured version (Figure 6A) shows even more inner features than the monomer (Figure 6B), which is mainly caused by the fact that the larger particles allow a more accurate image analysis. It is clear from Figure 6A,B that apart from a small protrusion near the central part of the dimer (indicated by the white arrow in Figure 6) the inner features of the left part of the dimer and the monomer are identical, confirming the same origin of both complexes. Two other rather common views lack a substantial amount of mass on either the right or left side (Figure 5 panels B and C, respectively) and represent 18% and 8% of the data set. Among the other dimeric projections, some lack this amount of mass on both sides (6% of the set, not shown) or are even more strongly reduced in size (Figure 5D, representing 2%

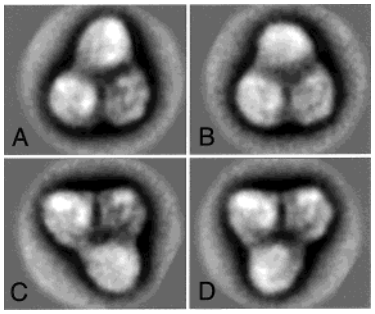

FIGURE 7: Classification of a set of 2000 trimeric aggregates of PSI-200. The four best classes (out of nine) are presented. Each class sum shows an additional PSI monomer associated with the PSI dimer as presented in Figure 5A, but in four different ways. In (A) and (B) the additional monomer is at two position on the upper side of the dimer, whereas in (C) and (D) the additional monomer is on the lower side. The number of summed images in A−D was 300, 175, 195, and 274, respectively.

of the data set). The right monomer is on the average embedded in a thicker layer of negative stain (see discussion), although in one class this difference was not very evident. In this class (Figure 5E), the upper right corner of the right monomer looks substantially larger than in the images of Figure 5A,C.

The two monomers of the dimer reveal a rather strong mirror-relatedness in projection, suggesting face-up and face-down orientations and, consequently, an artificial association of the two monomers. For such a pseudodimeric association only one type of handedness is expected, in agreement with the experimental results, because in this case a complete flip of the particle results in an identical projection. This is in contrast to native associations with only face-up or face-down associations, of which the PSII dimers and the cyanobacterial PSI trimers are good examples. The C_2S_2 PSII dimer has 2-fold rotational symmetry in the plane of the membrane, and a large set of isolated particles showed the presence of two types of mirror-related projections (*27*, *25*), though the numbers of face-down oriented particle projections are usually low. In the trimeric PSI complex of cyanobacteria the ratio of face-up and face-down was also rather variable; in our very first data set it was about 1:1 (*33*).

The fact that the two halves of the dimer are not totally identical in projection may be an artifact from the negative stain embedding, which tends to stain the top and the base of any molecule somewhat differently. This effect is enhanced by an overall stronger embedding of the right monomer in most of the projections, which is likely caused by the very asymmetric shape of the PSI molecule vertical to the membrane and may be enhanced by a slight tilting of the right monomer. An uneven stain embedding has also been shown for two-dimensional crystals packed with face-up and face-down oriented PSI monomers (*34*).

Trimers and Tetramers. Alignments and classification of the set of 2000 trimers resulted in four major class sums (Figure 7A−D). In each of these sums, three monomers are visible in positions that are clearly not related by 3-fold rotational symmetry. These trimers can therefore not be considered as native trimers and have no relationship to cyanobacterial trimers. The classification also indicates that the pseudotrimers form a heterogeneous set of particles. In

the best four classes, shown in Figure 7, the dimeric projection of Figure 5A is clearly visible in the lower two (Figure 7A,B) and upper two (Figure 7C,D) monomers. However, the third monomer is present in four different positions in Figure 7A−D with weak overall features, which indicates that the association of the third monomer is not very specific. In the omitted classes the fuzziness was even stronger.

The set of 436 tetrameric aggregates was also classified, but this set appeared to be too small to recognize predominant views with sufficient resolution, and the exact positions of the monomers could not be determined. It is very likely that a nonspecific association of the monomers is the main cause for the fuzziness. The association of the recently investigated heptameric aggregates of trimeric LHCII (*35*), for instance, is probably much better defined, since a significantly smaller data set than used for the analysis of the tetrameric PSI particles was sufficient to obtain a resolution of about 20 Å.

DISCUSSION

Artificial Aggregates. Dimers and higher aggregates or associations of PSI-200 have not been observed earlier. The two halves of the dimer appeared mirror-related in projection, and the monomeric units in the trimers and tetramers appeared not to be related by 3- or 4-fold symmetry. In addition, only one type of view was observed for the dimers. These features indicate that the observed dimers, trimers, and tetramers are composed of oppositely oriented units, and because it is highly unlikely that such units exist as such in the natural membranes, they must have come into existence by an artificial aggregation of detergent-solubilized monomers.

The artificial association is surprising given the fact that the aggregation must have occurred in a medium with large amounts of other solubilized protein complexes, such as ATP synthase, cytochrome b_6f, and trimeric and monomeric LHCII. The strong tendency of PSI-200 to form oppositely oriented dimers is most likely not a feature of the applied detergent (α-DM) and is also not specific for spinach. A partial solubilization of chloroplasts with Triton X-100 was also reported to give rise to an aggregation of PSI with oppositely oriented monomers (*9*, *10*), whereas a very similar dimeric association as in Figure 5A also occurred with PSI-200 complexes from *Arabidopsis thaliana* (E. J. Boekema, unpublished observations). We note that the existence of dimers, artificial or not, is advantageous for the EM analysis, because the increased size and the characteristic shape of the dimers allow a better alignment and classification of the complexes than the rather structureless monomers.

The resolution of the dimeric PSI single particles is on the order of 2−2.5 nm. This is somewhat lower than the resolution of the PSII supercomplex (maximally 1.65 nm), where within some of the five inner LHCII subunits (one trimer and two monomers) three stain-excluding masses could be deduced (*25*). Because the number of summed particles and the overall sizes are very comparable for both types of complexes, it could be that the lower resolution in PSI is caused by a somewhat more flexible dimeric association of the artificial PSI dimer than of the PSII dimer, for which there is clear evidence that this represents a native association (*25*).

Structural Organization of the PSI−LHCI Complex. The current resolution of the higher plant PSI complex allows a comparison with the structures from the well-resolved PSI complexes from cyanobacteria (which lack the LHCI antenna). The position of the reaction center part of PSI in cyanobacteria (Figure 6C) and higher plants (Figure 6A) is easily recognized since similar positions of densities can be observed in both structures (indicated by asterisks in Figure 6A,C). This implies that in the plant projection of Figure 6A, LHCI should be located at the lower half of the complex (Figure 6D), that the PSI-L subunit (which connects the three monomers in the cyanobacterial PSI trimer) should be located near the upper central part of the dimer (near the white arrow in Figure 6A), and that the PSI-F/J subunits (near the lowest asterisk in Figure 6C) should be located between the PSI-A/B and LHCI subunits. This orientation of the PSI core part in the PSI-200 complex implies that there should be a close connection between LHCI and the PSI-F/J subunits, which in cyanobacteria are peripherally located at the outer edge of the trimer and together consist of three transmembrane α-helices (*3*). Such a connection has not been revealed by cross-linking studies (*14*). On the other hand, the evidence is accumulating that the PSI-F/J subunits bind chlorophyll, both in cyanobacteria (*3*, *36*) and in green plants (*37*), suggesting that a location of PSI-F/J between LHCI and PSI-A/B does not have to interrupt the energy flow between these antenna units. Also the PSI-K subunit is probably located between the LHCI and PSI-A/B proteins (*38*).

The comparison of the higher plant and cyanobacterial PSI complexes also shows some other interesting similarities and differences. The mass of the domain involved in the trimerization of cyanobacterial PSI seems smaller than the mass in the corresponding position of the PSI-200 dimers (Figure 6D). This suggests additional mass in the green plant PSI, which may be explained by the PSI-H protein. This protein is not present in cyanobacteria and is located in the direct vicinity of PSI-L and PSI-I (*14*, *39*). We furthermore note that the cyanobacterial projection of Figure 6C was actually obtained from particles lacking the extrinsic subunits PSI-D and PSI-E. The α-DM-derived PSI particles, however, have full levels of both of these subunits (Figure 2), so there must be another factor that influences the internal features.

Size of the LHCI Antenna in PSI-200. The areas of the LHCI-containing parts of the PSI-200 dimer (Figure 6D) are about 95 and 75 nm^2 for the left and right parts of the dimer, respectively. The differences are probably caused by a possible tilting and heavier stain embedding of the right monomer. From the 4 Å LHCII crystal structure (*40*) it can be calculated that each trimeric LHCII unit occupies an area of about 40 nm^2. This implies that a monomeric LHCII unit occupies an area of 12−13 nm^2, and on the basis of the sequence similarities between all Cab proteins (*11*), it seems reasonable to assume that the LHCI proteins should occupy a very similar area. It thus appears that PSI-200 contains maximally 95/12 = 8 monomeric units of LHCI, in agreement with earlier estimations (*18*, *14*). However, the number of 8 could very well be lower if a nonoptimal packing of the LHCI complexes and/or a detergent contribution to the LHCI area in the PSI-200 complex has to be taken into account. It could, in this respect, be useful to compare the LHCI area in PSI-200 to the area of a LHCII/CP29/CP26 unit in the C_2S_2 PSII−LHCII supercomplex, which is known

to consist of one trimeric and two monomeric Cab proteins. The smallest LHCII/CP29/CP26 unit observed thus far occurs in Tris-washed PSII−LHCII supercomplexes (*41*), and in these complexes we calculate an area of about 105 nm^2, which is even larger than the LHCI area in PSI-200. It cannot be excluded, however, that there are more proteins in the LHCII/CP29/CP26 unit of the PSII−LHCII supercomplex. Recently, Ruf et al. (*42*) demonstrated the presence of a small chloroplast-encoded protein called LhbA, which is thought to consist of two transmembrane α-helices and which associates with CP26, and suggested that more such proteins may be present as well. Thus, if the LHCI and LHCII parts in PSI and PSII are equally packed and if there are no additional proteins in the LHCII part of PSII, the number of LHCI monomers in PSI-200 could be as low as $(5 \times 95)/105$, or 4−5. The uncertainty in packing, the unknown detergent contribution to the overall size, and the possible presence of more proteins in the PSII antenna, however, hamper a precise estimation.

The possibly lower numbers are in conflict with recent biochemical data, which point to a total of 10 monomeric LHCI proteins in each PSI-200 unit (*15*). We note, however, that the antenna size of the peripheral antenna in PSI-200 may not be very well defined. The EM analysis (Figure 5) revealed a substantial number of complexes of (slightly) smaller size, which probably lack a (small) part of the LHCI antenna, whereas the immunological analysis (Figure 2) revealed significant amounts of LHCI proteins in the later fractions of the gel-filtration chromatography, suggesting a partial release of all four LHCI proteins during solubilization and chromatography or the presence of a pool of unbound LHCI in the membranes.

Regardless of this uncertainty, however, the most conservative estimate suggests that the LHCI antenna in the complete PSI-200 complex should contain $180 - 100 = 80$ Chl ($a + b$) molecules, which together with the estimate of 10 Chl ($a + b$) molecules per LHCI monomer (*15*) suggests the presence of 8 LHCI monomers or 4 LHCI dimers. It cannot be excluded, however, that some of the chlorophylls are located at the interface between the LHCI units or between LHCI and the PSI core (*13*) and that during the purification procedures of LHCI such chlorophylls are lost, implying that lower numbers of LHCI proteins in each PSI-200 complex (such as 6 LHCI monomers or 3 LHCI dimers) are also possible on the basis of these biochemical considerations.

Trimer Formation in Plant PSI. A very important point is that the presence of LHCI in the higher plant PSI does not cause any structural hindrances for the formation of a similar type of trimer as observed in cyanobacteria (Figure 6D). To our knowledge, native trimers with similarly oriented subunits of higher plant PSI-200 complexes have never been found. It is possible that other factors than the binding of LHCI (such as the presence of the PSI-H protein) prevent trimer formation. It cannot be excluded, however, that under certain physiological conditions such trimeric complexes do occur in vivo but remained undetected thus far and that the trimeric organization (or the possibility of the photosynthetic organism to change between monomeric and trimeric organization forms) is a general phenomenon of PSI in all photosynthetic organisms.

ACKNOWLEDGMENT

We thank Dr. W. Keegstra for his help with image processing and Marianne Cetin for her help with the P700 measurements.

REFERENCES

1. Wollman, F.-A., Minai, L., and Nechustai, R. (1999) *Biochim. Biophys. Acta 1411*, 21−85.
2. Krauss, N., Schubert, W.-D., Klukas, O., Fromme, P., Witt, H. T., and Saenger, W. (1996) *Nat. Struct. Biol. 3*, 965−973.
3. Schubert, W.-D., Klukas, O., Krauss, N., Saenger, W., Fromme, P., and Witt, H. T. (1997) *J. Mol. Biol. 272*, 741−769.
4. Westermann, M., Neuschaefer-Rube, O., Mörschel, E., and Wehrmeyer, W. (1999) *J. Plant Physiol. 155*, 24−33.
5. Boekema, E. J., Dekker, J. P., van Heel, M. G., Rögner, M., Saenger, W., Witt, I., and Witt, H. T. (1987) *FEBS Lett. 217*, 283−286.
6. Kruip, J., Chitnis, P. R., Lagoutte, B., Rögner, M., and Boekema, E. J. (1997) *J. Biol. Chem. 272*, 17061−17069.
7. Bald, D., Kruip, J., and Rögner, M. (1996) *Photosynth. Res. 49*, 103−118.
8. Karapetyan, N. V., Holzwarth, A. R., and Rögner, M. (1999) *FEBS Lett. 460*, 395−400.
9. Kitmitto, A., Holzenburg, A., and Ford, R. C. (1997) *J. Biol. Chem. 272*, 19497−19501.
10. Kitmitto, A., Mustafa, A. O., Holzenburg, A., and Ford, R. C. (1998) *J. Biol. Chem. 273*, 29592−29599.
11. Jansson, S. (1994) *Biochim. Biophys. Acta 1184*, 1−19.
12. Knoetzel, J., Svendsen, I., and Simpson, D. J. (1992) *Eur. J. Biochem. 206*, 209−215.
13. Schmid, V. H. R., Cammarata, K. V., Bruns, B. U., and Schmidt, G. W. (1997) *Proc. Natl. Acad. Sci. U.S.A. 94*, 7667−7672.
14. Jansson, S., Andersen, B., and Scheller, H. V. (1996) *Plant Physiol. 112*, 409−420.
15. Croce, R., and Bassi, R. (1998) in *Photosynthesis: Mechanisms and Effects* (Garab, G., Ed.) pp 421−424, Kluwer Academic Publishers, Dordrecht, The Netherlands.
16. Ihalainen, J. A., Gobets, B., Sznee, K., Brazzoli, M., Croce, R., Bassi, R., van Grondelle, R., Korppi-Tommola, J. E. I., and Dekker, J. P. (2000) *Biochemistry 39*, 8625−8631.
17. Kühlbrandt, W., Wang, D. N., and Fujiyoshi, Y. (1994) *Nature 367*, 614−621.
18. Boekema, E. J., Wynn, R. M., and Malkin, R. (1990) *Biochim. Biophys. Acta 1017*, 49−56.
19. Okkels, J. S., Scheller, H. V., Svendsen, I., and Möller, B. L. (1991) *J. Biol. Chem. 266*, 6767−6773.
20. Chitnis, V. P., Xu, Q., Yu., L., Golbeck, J. H., Nakamoto, H., Xie, D. L., and Chitnis, P. R. (1993) *J. Biol. Chem. 268*, 11678−11684.
21. Chitnis, V. P., and Chitnis, P. R. (1993) *FEBS Lett. 336*, 330−334.
22. Van Roon, H., van Breemen, J. F. L., de Weerd, F. L., Dekker, J. P., and Boekema, E. J. (2001) *Photosynth. Res. 64*, 155−166.
23. Porra, R. J., Thompson, W. A., and Kriedemann, P. E. (1989) *Biochim. Biophys. Acta 975*, 374−384.
24. Lüneberg, J., Fromme, P., Jekow, P., and Schlodder, E. (1994) *FEBS Lett. 338*, 197−202.
25. Boekema, E. J., van Roon, H., Calkoen, F., Bassi, R., and Dekker, J. P. (1999) *Biochemistry 38*, 2233−2239.
26. Harauz, G., Boekema, E., and van Heel, M. (1988) *Methods Enzymol. 164*, 35−49.
27. Boekema, E. J., Hankamer, B., Bald, D., Kruip, J., Nield, J., Boonstra, A. F., Barber, J., and Rögner, M. (1995) *Proc. Natl. Acad. Sci. U.S.A. 92*, 175−179.
28. Van der Lee, J., Bald, D., Kwa, S. L. S., van Grondelle, R., Rögner, M., and Dekker, J. P. (1993) *Photosynth. Res. 35*, 311−321.

29. Ke, B. (1972) *Arch. Biochem. Biophys. 152*, 70−77.
30. Pålsson, L.-O., Flemming, C., Gobets, B., van Grondelle, R., Dekker, J. P., and Schlodder, E. (1998) *Biophys. J. 74*, 2611−2622.
31. Malkin, R., Ortiz, W., Lam, E., and Bonnerjea, J. (1985) *Physiol. Veg. 23*, 619−625.
32. Boekema, E. J., van Roon, H., and Dekker, J. P. (1998) *FEBS Lett. 424*, 95−99.
33. Boekema, E. J., Dekker, J. P., Rögner, M., Witt, I., Witt, H. T., and van Heel, M. (1989) *Biochim. Biophys. Acta 974*, 81−87.
34. Böttcher, B., Gräber, P., and Boekema, E. J. (1992) *Biochim. Biophys. Acta 1100*, 125−136.
35. Dekker, J. P., van Roon, H., and Boekema, E. J. (1999) *FEBS Lett. 449*, 211−214.
36. Soukoulis, V., Savikhin, S., Xu, W., Chitnis, P. R., and Struve, W. S. (1999) *Biophys. J. 76*, 2711−2715.
37. Tjus, S. E., Roobol-Boza, M., Pålsson, L.-O., and Andersson, B. (1995) *Photosynth. Res. 45*, 41−49.
38. Jensen, P. E., Gilpin, M., Knoetzel, J., and Scheller, H. V. (2000) *J. Biol. Chem. 275*, 24701−24708.
39. Naver, H., Haldrup, A., and Scheller, H. V. (1999) *J. Biol. Chem. 274*, 10784−10789.
40. Kühlbrandt, W. (1994) *Curr. Opin. Struct. Biol. 4*, 519−528.
41. Boekema, E. J., van Breemen, J. F. L., van Roon, H., and Dekker, J. P. (2000) *Biochemistry 39*, 12907−12915.
42. Ruf, S., Biehler, K., and Bock, R. (2000) *J. Cell Biol. 149*, 369−377.

BI0015358